Minibeam radiation therapy enhanced tumor delivery of PEGylated liposomal doxorubicin in a triple-negative breast cancer mouse model

Ther Adv Med Oncol

2021, Vol. 13: 1–14

DOI: 10.1177/17588359211053700

Lauren S.L. Price*, Judith N. Rivera*, Andrew J. Madden, Leah B. Herity, Joseph A. Piscitelli, Savannah Mageau, Charlene M. Santos, Jose R. Roques, Bentley Midkiff, Nana N. Feinberg, David Darr, Sha X. Chang† and William C. Zamboni†

Abstract

Background: Minibeam radiation therapy is an experimental radiation therapy utilizing an array of parallel submillimeter planar X-ray beams. In preclinical studies, minibeam radiation therapy has been shown to eradicate tumors and cause significantly less damage to normal tissue compared to equivalent radiation doses delivered by conventional broadbeam radiation therapy, where radiation dose is uniformly distributed.

Methods: Expanding on prior studies that suggested minibeam radiation therapy increased perfusion in tumors, we compared a single fraction of minibeam radiation therapy (peak dose:valley dose of 28 Gy:2.1 Gy and 100 Gy:7.5 Gy) and broadbeam radiation therapy (7 Gy) in their ability to enhance tumor delivery of PEGylated liposomal doxorubicin and alter the tumor microenvironment in a murine tumor model. Plasma and tumor pharmacokinetic studies of PEGylated liposomal doxorubicin and tumor microenvironment profiling were performed in a genetically engineered mouse model of claudin-low triple-negative breast cancer (T11).

Results: Minibeam radiation therapy (28 Gy) and broadbeam radiation therapy (7 Gy) increased PEGylated liposomal doxorubicin tumor delivery by 7.1-fold and 2.7-fold, respectively, compared to PEGylated liposomal doxorubicin alone, without altering the plasma disposition. The enhanced tumor delivery of PEGylated liposomal doxorubicin by minibeam radiation therapy is consistent after repeated dosing, is associated with changes in tumor macrophages but not collagen or angiogenesis, and nontoxic to local tissues. Our study indicated that the minibeam radiation therapy's ability to enhance the drug delivery decreases from 28 to 100 Gy peak dose.

Discussion: Our studies suggest that low-dose minibeam radiation therapy is a safe and effective method to significantly enhance the tumor delivery of nanoparticle agents.

Keywords: microbeam radiation, nanoparticle, pharmacokinetics, tumor delivery, tumor microenvironment

Received: 15 September 2019; revised manuscript accepted: 29 September 2021.

Correspondence to:
William C. Zamboni
Division of Pharmacotherapy & Experimental Therapeutics, UNC Eshelman School of Pharmacy, The University of North Carolina at Chapel Hill, 1022B Genetic Medicine Building, 120 Mason Farm Road, Campus Box 7361, Chapel Hill, NC 27599-7361, USA

Translational Oncology and Nanoparticle Drug Development (TOND2I) Lab, The University of North Carolina at Chapel Hill, Chapel Hill, NC, USA

UNC Lineberger Comprehensive Cancer Center, Chapel Hill, NC, USA

Carolina Center of Cancer Nanotechnology Excellence (C-CCNE), Chapel Hill, NC, USA

North Carolina Biomedical Innovation Network, The University of North Carolina at Chapel Hill, Chapel Hill, NC, USA
zamboni@email.unc.edu

Lauren S.L. Price
Andrew J. Madden
Leah B. Herity
Joseph A. Piscitelli
Division of Pharmacotherapy & Experimental Therapeutics, UNC Eshelman School of Pharmacy, Chapel Hill, NC, USA

Translational Oncology and Nanoparticle Drug Development (TOND2I) Lab, The University of North Carolina at Chapel Hill, Chapel Hill, NC, USA

Introduction

The theoretical advantages of carrier-mediated agents (CMAs) in cancer treatment include increased solubility, prolonged duration of exposure, selective delivery of entrapped drug to the tumor, and an improved therapeutic index.[1,2] The primary types of anticancer CMAs are liposomes, nanoparticles (NPs), and conjugated agents. PEGylated liposomal doxorubicin (PLD), liposomal daunorubicin (DaunoXome®), and paclitaxel albumin-bound particles (Abraxane®) are members of this relatively new class of drugs

Savannah Mageau
Division of Pharmacotherapy & Experimental Therapeutics, UNC Eshelman School of Pharmacy, Chapel Hill, NC, USA

UNC Advanced Translational Pharmacology and Analytical Chemistry (ATPAC) Lab, The University of North Carolina at Chapel Hill, Chapel Hill, NC, USA

Judith N. Rivera
Joint Department of Biomedical Engineering, The University of North Carolina at Chapel Hill and North Carolina State University, Chapel Hill, NC, USA

Charlene M. Santos
Jose R. Roques
UNC Lineberger Comprehensive Cancer Center, Chapel Hill, NC, USA

The Animal Studies Core, UNC at Chapel Hill, Chapel Hill, NC, USA

Bentley Midkiff
Nana N. Feinberg
Translational Pathology Lab, UNC Lineberger Comprehensive Cancer Center, Chapel Hill, NC, USA

David Darr
UNC Lineberger Comprehensive Cancer Center, Chapel Hill, NC, USA

Sha X. Chang
Joint Department of Biomedical Engineering, The University of North Carolina at Chapel Hill and North Carolina State University, Chapel Hill, NC, USA

UNC Lineberger Comprehensive Cancer Center, Chapel Hill, NC, USA

Department of Radiation Oncology, UNC at Chapel Hill, Chapel Hill, NC, USA

*These authors contributed equally to this work and should be considered co-first authors.

†These senior co-authors contributed equally to this work.

that are approved by the US FDA for the treatment of solid tumors.[3] However, the promise of these drugs is currently unfulfilled due to an overall low tumor uptake.[4,5] In theory, enhancing permeability of the tumor vasculature allows CMAs to enter the tumor interstitial space, while suppressed lymphatic filtration allows them to stay there. This phenomenon, termed the Enhanced Permeability and Retention (EPR) effect, may be exploited by CMAs to deliver drugs to tumors.[4,5] However, progress in developing effective CMAs using this approach has been hampered by heterogeneity of EPR effect in different tumors and the lack of information on factors that influence EPR.[4–7] In addition, cancer cells in tumors are surrounded by a complex microenvironment comprised of endothelial cells of the blood and lymphatic circulation, stromal fibroblasts, collagen, cells of the mononuclear phagocyte system (MPS), and other immune cells that may be associated with the variability in EPR and are potential barriers to tumor delivery of CMAs.[4,6–12] Moreover, it appears that the ability of CMAs to enter tumors by EPR or other factors is highly variable across tumor types and thus all solid tumors may not be conducive for CMA delivery and treatment.[4,8,13–19] It is also unclear how these factors affect CMAs of different sizes and shapes.[13,20,21] Thus, it is important to development of new methods to overcome barriers and increase the tumor delivery of several different types of CMAs in solid tumors with different degrees of EPR effect.

The pharmacokinetics (PK) of CMAs is dependent on the carrier and not the encapsulated drug it carries.[8,10,14,17] Drug that remains encapsulated within the carrier has a completely different clearance and distribution compared with small molecule (SM) drugs, including enhanced delivery of the carrier to the tumor. However, PK studies show that in reality the tumor delivery of CMAs is low and inefficient due to tumor heterogeneity and associated barriers.[8,10,14,17] Recent publications have highlighted the relatively lower efficiency of tumor delivery seen with CMAs compared with SMs. In addition, a workshop by the Alliance for Nanotechnology in Cancer concluded that there are major gaps in the understanding of factors that affect and inhibit CMA and NP tumor delivery, and new fundamental preclinical and clinical studies in this area are needed to effectively advance CMA and NP drug delivery and efficacy in solid tumors.[4,22] So far, the advancement of CMA and NP treatment of cancer has been focused primarily on modifying formulations to overcome PK, efficacy, and toxicity issues. However, this approach alone may not be adequate as biologic issues, such as barriers within the tumor microenvironment appear to play important roles in low and inefficient tumor delivery of CMAs.

Radiation therapy has been used for cancer local control in more than half of cancer patients in North America.[23] Cytotoxic radiation is targeted at the tumor and causes tumor cell DNA double strand breaks, which lead to cell death and then tumor control. Although radiation is effective in tumor control, the risk of unacceptable collateral radiation damage to the surrounding normal tissue, especially that of nearby critical organs, often prevents radiation oncologists from prescribing the high radiation dose needed for tumor control. We have only recently begun to understand the effects of radiation on cells beyond the cytotoxic effect, such as the bystander effect, the abscopal effect, tumor microenvironment modulation, and radiation-induced anticancer immune responses.[24–26] Although these effects remain poorly understood, they promise new paths for using radiation to treat cancer.[25,27,28]

Minibeam radiation therapy (MBRT) is used in this work and it belongs to a nonconventional form of radiation therapy often referred to as spatially fractionated radiation therapy (SFRT).[29] MBRT[30] and microbeam radiation therapy (MRT)[31] are both forms of SFRT used in preclinical studies while the clinical forms of SFRT include GRID therapy[32,33] and Lattice therapy.[34] Although they differ in geometric and dosimetric scale, all forms of SFRT may be characterized by unique, repeated dose patterns consisting of many small, high-dose subregions separated by larger, low-dose subregions.[29] For instance, 'spatially fractionated' dose distributions may include high ('peak') dose subregions that are on the order of 50 μm wide for MRT, 300 μm for MBRT, and 1 cm wide for GRID and Lattice therapy. Although X-ray radiation has been traditionally used for SFRT, protons are a new source of radiation that is ideal for SFRT.[35] We hypothesize that all forms of SFRT may share similar basic working mechanisms. Although a specific finding from a study using one form of SFRT may not be directly translatable to another form initially, it may be possible to translate the findings after applying appropriate adjustments in geometric and dosimetric scale. We have previously

characterized some of the unique dosimetric parameters of different forms of SFRT (including MBRT, the form of SFRT used in this work) and their correlations with treatment responses in a recent preclinical study.[36] In animal studies, high-dose MRT and MBRT have shown an extremely high tissue-type selectivity, eradicating tumors without damaging or inhibiting the function of normal tissues that are exposed to the same high-dose radiation.[25,27] The extraordinary M(B)RT effect may stem from its unique spatial and dosimetric characteristics, which are radically different than those of conventional broadbeam radiation therapy (BRT). MRT consists of many parallel microplanar beams at peak dose levels that are 10–100 times greater than BRT.[27] Compared with MRT, MBRT employs a larger scale planar beam width of several hundred microns.[36] Consequently, MBRT beams may be generated using any one of the widely available small animal X-ray irradiators, which makes its study more relevant to potential clinical translation and application as compared with MRT, which is typically generated only at a handful of synchrotron facilities around the world.[37] Remarkably, in animal studies, the ultrahigh M(B)RT dose (several hundred Gy peak dose) is well tolerated by normal tissue while producing tumor control and survival comparable to conventional BRT. The working mechanism for M(B)RT normal tissue-sparing effect is not fully understood and the hypotheses include (1) surviving stem cells in the low dose M(B)RT valley regions repopulate and repair tissue damage and (2) its mature microvasculature is resistant to M(B)RT damage.[29] The mechanism of M(B)RT tumor control is still poorly understood,[29] but hypotheses include (1) cellular bystander effect where unirradiated or less-irradiated cells in the beam valley regions are exposed to the cytotoxic factors released by nearby dying cells in the beam peak regions that received massive radiation dose, (2) the immature tumor microvasculature is prone to damage by the high-dose M(B)RT, and (3) radiation-induced immune responses.[29] In addition to these direct impacts on tumor control, M(B)RT may also alter the tumor microenvironment factors important to the delivery of CMAs. Griffin *et al.*[29] reported that MRT induced a transient but drastic reduction in tumor hypoxia which might open up vessels for better drug delivery. We hypothesize that improving tumor delivery of CMAs with low toxicity makes MBRT an attractive combination therapy for multimodal cancer treatment.

Methods

Animal model

All animal studies were completed under a protocol approved by the University of North Carolina at Chapel Hill Institutional Animal Care and Use Committee (UNC IACUC #20-177.0-A) and in accordance with all relevant animal welfare regulations. Mice were maintained in a barrier facility on a 12 h light/dark cycle and were provided with folate-free chow and water ad libitum. Tumors derived from BALB/c TP53−/− orthotopic mammary gland transplant line (T11) were transplanted into the inguinal mammary fat pad of 12-week-old female BALB/cJ mice (The Jackson Laboratory; strain 000651).[16,38,39] Mice were housed in the UNC Lineberger Comprehensive Cancer Center's Mouse Phase I Unit and observed for tumors as per the standard practice.[40] Mice were randomized to treatment cohorts, and therapy began once a tumor reached approximately 300–500 mm^3.

Radiation treatments

An XRAD-320 Research Irradiator (Precision X-Rays, Inc.; North Branford, CT) using the 160 kVp energy and 25 mA current settings as well as added 0.254 mm Cu filtration was used to generate the MBRT radiation used in this work. Customized radiation collimators were used to produce both the BRT (uniform radiation) and MBRT (co-planar beams arrangement) fields. Figure 1 shows an example of the animal irradiation and MBRT dosimetry. Radiation dosimetry for both the BRT and MBRT treatments was determined via EBT3 Gafchromic film calibrated with an ion chamber under broad field conditions, in accordance with the American Association of Physicists in Medicine (AAPM) Task Group Report No. 061, 'AAPM Protocol for 40–300 kV x-ray beam dosimetry in radiotherapy and radiobiology'. The in-house developed MBRT collimator generated 307 μm-wide beams (measured full-width-at-half-maximum, averaged for each peak) that were spaced approximately 1260 μm apart (average peak-to-peak distance). The average MBRT peak-to-valley dose ratio (PVDR) at the surface for our setup was approximately 13.3 and the skin surface dose rates used for treatments varied from 1.73 to 2.5 Gy per minute for MBRT (averaged for each peak) and BRT, respectively. The dose rate for the MBRT radiation treatment was approximately 3 Gy/min,

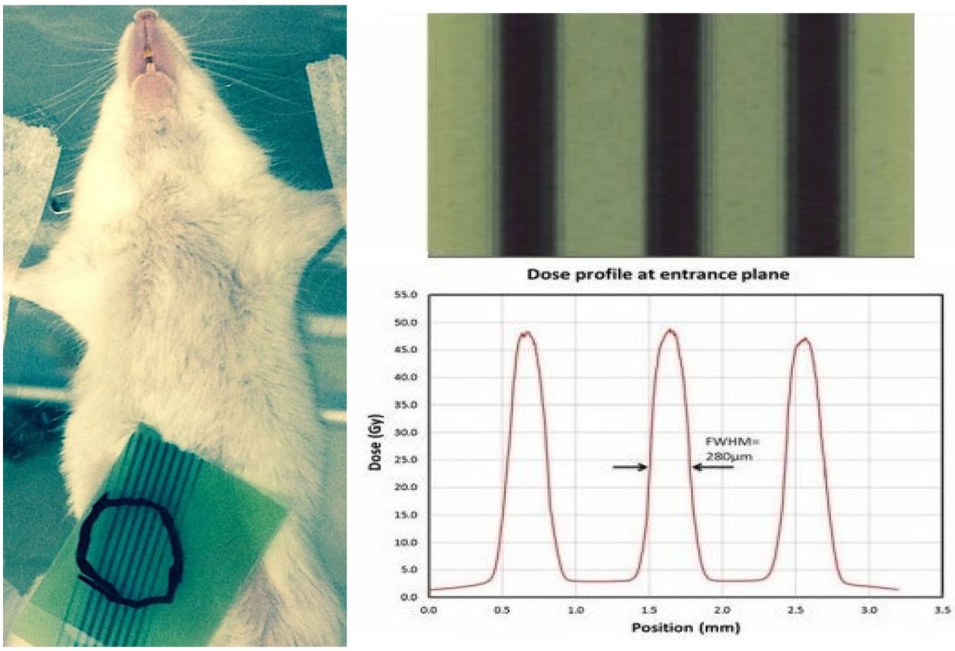

Figure 1. An example MBRT irradiation (left) where the targeted irradiation area entered around the tumor (invisible) is marked on the treatment verification film placed on top the animal during treatment. Sample MBRT dosimetry EBT film (top right) and dose profile (bottom right) on the surface of a 2 cm × 2 cm phantom. The average peak width is 280 μm and valley width is 1000 μm. The PVDR is in the range of 10 in this study (note that PVDR is larger when fewer peaks are used as in the film measurement with only three peaks used).

which is similar to the dose rate used in conventional radiation therapy patient treatment.

PK studies

The number of mice, study design, and sampling scheme for the PK studies evaluated here are standard for PK studies of NP, PLD, and used by our group and others for PK studies of these agents in mice.[16,41,42] Mice were anesthetized using isoflurane and treated with BRT 7 Gy, MBRT 28 Gy, or MBRT 100 Gy. Following completion of radiation, mice were returned to the vivarium and monitored for signs of toxicity. Mice were administered PLD at 6 mg/kg IV ×1 via a tail vein at 24 h after BRT at 7 Gy, MBRT at 28 Gy, or MBRT at 100 Gy. An additional group of mice with no radiation exposure were also administered an identical dose of PLD. At predefined time points following PLD administration (5 min, 24 h, and 96 h), mice were anesthetized using 100 mg/kg ketamine IP ×1 and 1 mg/kg dexmedetomidine IP ×1 and then sacrificed via cardiac puncture for collection of blood. Tumors were excised postmortem and snap frozen in liquid nitrogen and stored at −80°C until processing. At each sampling time point in each study, plasma and tumor samples were obtained from $n = 3$ mice, which is standard for plasma and tumor PK studies in mice.

To evaluate the effects of multiple treatments of MBRT, additional animals received a second treatment of MBRT 28 Gy (on day 8) + PLD at 6 mg/kg IV (on day 9 at 24 h after MBRT) 1 week after the initial treatment (MBRT on day 1 and PLD on day 2 at 24 h post MBRT). Mice ($n = 3$ per time point) were sacrificed 5 min and 24 h following the second dose of PLD and blood and tissues collected as above. The time points for the multidose study were based on the results of the single-dose studies of MBRT at 28 Gy + PLD compared with PLD alone.

PLD analytical studies

PLD was purchased from FormuMax Scientific and diluted with 5% dextrose in water to 1.2 mg/ml before injection. The complete methods for sample collection, preparation and analysis of encapsulated doxorubicin in plasma, and sum total (encapsulated + released) doxorubicin in tumor after administration of PLD have been

previously described.[16,43–47] Briefly, blood samples were collected in sodium heparin tubes after the administration of PLD. Blood was centrifuged at 1500*g* for 5 min to obtain plasma. Encapsulated and released doxorubicin in plasma were separated using solid-phase separation. Upon processing, tumors were thawed, weighed, and diluted in a 1:3 ratio with phosphate-buffered saline prior to homogenizing with a Precellys 24 bead mill homogenizer (Omni International Inc, Kennesaw, GA). Samples were further processed by addition of 800 µl extraction solution (acetonitrile with 100 ng/ml daunorubicin internal standard) to 200 µl of plasma or tumor homogenate. The samples were vortexed for 10 min and centrifuged at 10,000*g* for 10 min at 4°C. The supernatant was removed to a clean tube, evaporated to dryness under nitrogen, and reconstituted in 150 µl of 15% acetonitrile in water plus 0.1% formic acid. The samples were then vortexed, transferred to autosampler vials, and analyzed by high-performance liquid chromatography with fluorescence detection (HPLC-FL) set to excitation wavelength 490 nm/emission wavelength 590 nm. The HPLC-FL technique had a quantitative range of 10 – 3,000 ng/ml for sum total doxorubicin in tumor and 300–30,000 ng/ml for encapsulated doxorubicin in plasma. Samples that returned a concentration above the quantitative limit were diluted to fall within the quantitative range and reinjected.

PK analysis

Destructive sampling methods and groupings were used to generate the PK parameters, where the plasma and tumor concentration *versus* time values in each treatment cohort were grouped together to generate a single mean value at each time point and subsequent single PK parameter.[16,41,42] The mean concentration *versus* time PLD plasma and tumor for each cohort was analyzed by noncompartmental analysis using Phoenix WinNonlin Professional Edition version 8.0 (Pharsight Corp., Cary, NC, USA). The area under the doxorubicin concentration *versus* time curve (AUC) was calculated using the linear up/log down rule for plasma and tumor from 0 to T_{last} (24 or 96 h, depending on treatment group).

Tumor staining and immunohistochemistry (IHC)

A separate group of T11 mice ($n = 4$ per treatment group) were randomized to either no radiation, BRT 7 Gy, MBRT 28 Gy, or MBRT 100 Gy and irradiated as above. At 24 h after radiation, mice were anesthetized with ketamine and dexmedetomidine and sacrificed by cervical dislocation. The use of $n = 4$ mice per time point is based on our prior tumor profiling studies in the T11 tumor model. Tumors were excised postmortem and placed into 10% formaldehyde for paraffin embedding. Tumors were then sliced and mounted on slides for staining. Samples were stained using Masson's Trichrome Stain (MTS), anti-Collagen IV monoclonal antibody, anti-F4/80 monoclonal antibody, and anti-CD31 monoclonal antibody as previously described.[16]

Stained slides were scanned using ScanScope XT (Leica Biosystems Inc.), an Automated High-Throughput Scanner. A quantifying algorithm employing a modified membrane analysis was utilized to automatically quantify the stained area of viable tumor.[16] Collagen IV, MTS, and macrophages (F4/80) in the viable tumor tissue were quantified by standard H-score. Microvessels (CD31) were quantified by microvessel density ($1/mm^2$).[16,48]

Statistical analysis

Statistical analyses were carried out using SAS v.9.2 (Cary, NC) and Prism5 software (GraphPad Software, Inc.).[49] Analysis of covariance (ANCOVA) was performed followed by adjustment for multiple comparisons using Holm test to test for differences in tumor volume, plasma concentrations at each time point, tumor concentrations at each time point, and TME factors among all treatment groups.[50] p value of less than 0.05 was considered statistically significant. All statistical tests were two-sided.

Results and discussion

Overview

In order to assess the impact of MBRT on the tumor delivery enhancement of CMAs, we evaluated the PK of PLD in a genetically engineered mouse model of triple-negative breast cancer (T11) following either MBRT or conventional BRT. Radiation-enhanced accumulation of NPs and macromolecules in tumors has been reported in several previous studies.[51–57] However, this is the first publication comparing the impact of conventional BRT and the novel MBRT on the tumor microenvironment and the tumor accumulation of

a drug-loaded NP. We also evaluated the impact of MBRT on the tumor microenvironment through histological examination of tumor in irradiated animals.

Single-dose PK

We first evaluated the PK of PLD in tumor-bearing T11 mice following a single dose of either PLD alone, BRT 7 Gy + PLD, MBRT 28 Gy + PLD, or MBRT 100 Gy + PLD. In the remaining two combination therapy arms (BRT 7 Gy + PLD and MBRT 100 Gy + PLD), radiation was administered 24 h prior to PLD. The encapsulated doxorubicin plasma and sum total tumor doxorubicin concentration *versus* time profiles for all single dose treatments are presented in Figure 2. The encapsulated plasma and sum total tumor doxorubicin $AUC_{0\text{-}96h}$ and ratio of tumor to plasma $AUC_{0\text{-}96h}$ are presented in Table 1.

The encapsulated plasma concentration *versus* time profiles and $AUC_{0\text{-}96h}$ did not significantly differ between treatments. Because the irradiated area in this study was limited to a relatively small area centered on the tumor mass, little impact was anticipated on the primary clearance pathway of NPs—the MPS. Consistent with this hypothesis, the plasma exposure of PLD was similar across all groups (<25% difference in $AUC_{0\text{-}96h}$), regardless of radiation type or dose, suggesting that a single dose of BRT or MBRT minimally alters the plasma clearance and disposition of PLD.

In contrast, all BRT and MBRT treatment groups had significantly higher sum total tumor doxorubicin exposure compared with PLD alone. The sum total tumor doxorubicin $AUC_{0\text{-}96h}$ were 2.7-fold and 2.2-fold higher following BRT 7 Gy and MBRT 100 Gy, respectively, compared with PLD alone. MBRT 28 Gy yielded the highest PLD tumor delivery enhancement with a tumor $AUC_{0\text{-}96h}$ 6.3-fold higher compared with PLD alone.

The tumor:plasma doxorubicin AUC ratio represents the relative delivery of NPs to tumor compared with the plasma. Tumor delivery results following radiation therapy mirrored the tumor exposure due to the limited impact of radiation on the plasma exposure. The ratio of tumor to plasma $AUC_{0\text{-}96h}$ were 2.7-fold, 7.1-fold, and 2.8-fold higher following BRT 7 Gy, MBBRT 28 Gy, and MBRT 100 Gy, respectively, compared with PLD alone. These results show that MBRT provides comparable enhancement of tumor NP accumulation to BRT when given at ~14 times the peak dose (i.e. MBRT 100 Gy was similar to BRT 7 Gy). Despite increased peak doses, MBRT typically has significantly lower normal tissue toxicity when compared with BRT while maintaining antitumor efficacy.[27] The combination of independent antitumor activity, low normal tissue adverse effects, and comparable tumor delivery enhancement makes MBRT an attractive modality for combination therapy in this manner.

Intriguingly, the lower peak radiation dose (MBRT 28 Gy) provided the most significant enhancement of tumor drug delivery following a single dose, suggesting that the relationship between radiation dose and tumor delivery enhancement may not be proportional. This observation is consistent with our previous study of MBRT on tumor vasculature modulation in a window chamber tumor model.[25] While the administration of BRT 7 Gy + PLD enhanced the relative delivery of PLD to the tumor 2.7-fold compared with PLD alone, MBRT 28 Gy + PLD enhanced the relative delivery of PLD a further 2.6-fold compared with BRT 7 Gy + PLD. Similarly, MBRT 28 Gy + PLD enhanced relative delivery of PLD to tumor 2.5-fold compared with MBRT 100 Gy + PLD, which itself provided 2.8-fold enhancement relative to PLD alone.

In all of the PK and tumor profiling studies, the tumors in each mouse were between 150 and 300 mm^3 in size. However, after the PK samples were collected from the study evaluating the PLD PK at 96 h after MBRT at 28 Gy, it was determined that the mice ($n = 3$) had smaller tumors ($75.3 \pm 0.6\ mm^3$). Thus, these PK studies were repeated in mice ($n = 3$) with standard sized tumors ($210.3 \pm 52.8\ mm^3$). Having PK results in these two groups of mice allowed us to evaluate the relationship between tumor size, plasma exposure of PLD, and tumor exposure of PLD mediated by MBRT. The tumor size, encapsulated plasma doxorubicin concentration, sum total tumor concentration, and tumor to plasma concentration ratio for these animals are presented in Table 2.

The mice with the smaller tumors ($75.3 \pm 0.6\ mm^3$) had the higher plasma doxorubicin exposure and the mice with the larger tumors ($210.3 \pm 52.8\ mm^3$) had the lower plasma doxorubicin exposure. These results are consistent with mice with larger tumors having enhanced clearance of NP agents.[58,59] Higher plasma exposure led to higher

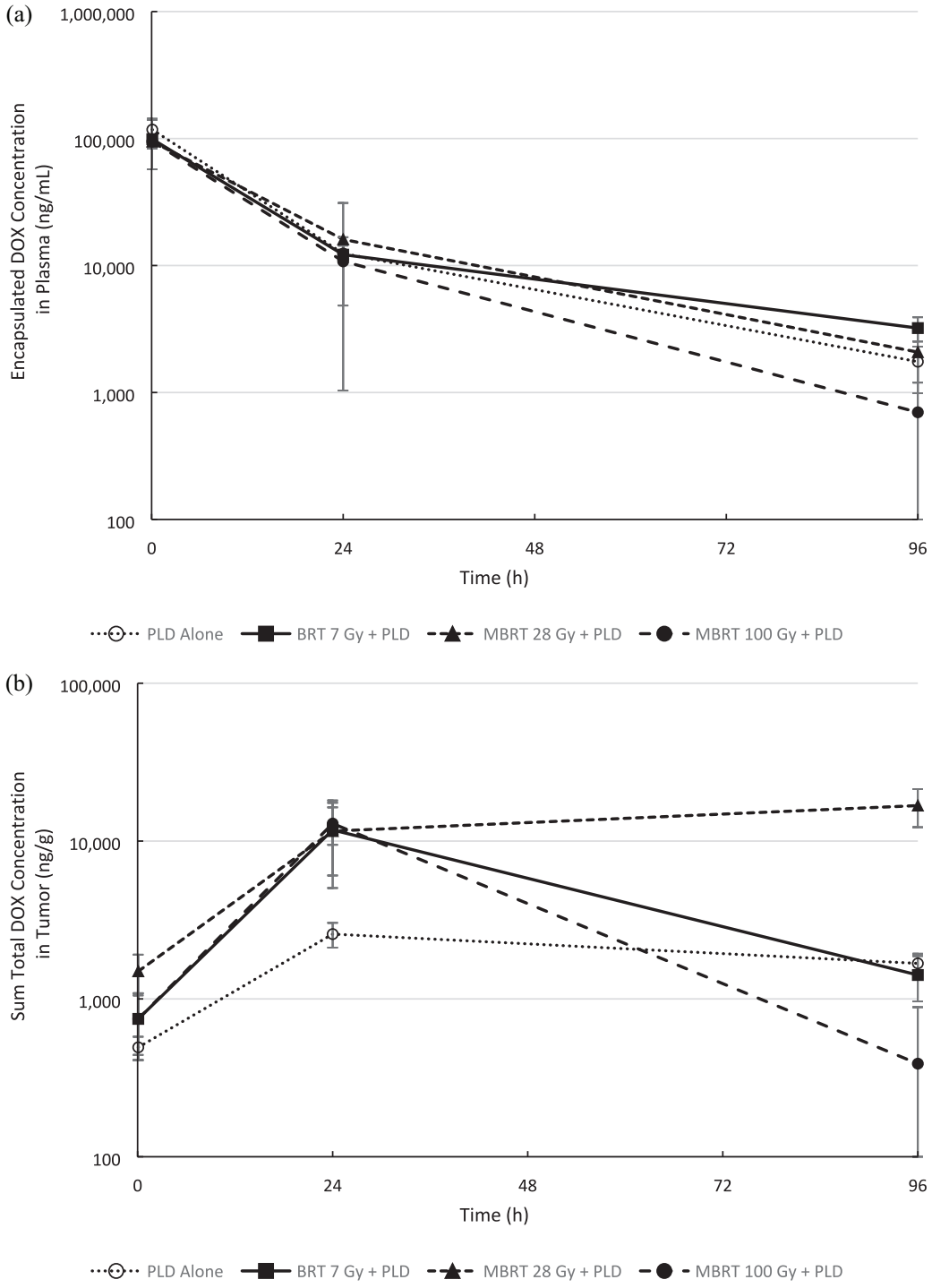

Figure 2. Mean and SD encapsulated doxorubicin concentration in plasma (a) and sum total doxorubicin concentration in tumor (b) *versus* time profiles in female T11 mice after administration of: (1) PLD 6 mg/kg alone, (2) BRT 7 Gy + PLD, (3) MBRT 28 Gy + PLD, or (4) MBRT 100 Gy + PLD. Plasma and tumor samples in these studies were obtained prior to administration and at 5 min, 24 h, and 96 h after PLD administration. The encapsulated doxorubicin exposure in plasma is similar at all time points and among all groups ($p > 0.05$), which is consistent with a lack of effect of irradiation on plasma clearance of PLD. The tumor exposure of sum total doxorubicin is significantly enhanced at 24 h post-PLD for all radiation therapy groups compared with PLD alone ($p < 0.05$). At 96 h post-PLD, the tumor exposure was significantly higher in the MBRT 28 Gy + PLD cohort compared with all other groups, which were not statistically different ($p > 0.05$). Overall, from 0 to 96 h the greatest increase in tumor exposure of sum total doxorubicin was after treatment with MBRT 28 Gy + PLD 6 mg/kg as compared with all other groups.

Table 1. Summary of PLD pharmacokinetics after a single dose of PLD alone, BRT + PLD, or MBRT + PLD.

PK parameter	PLD alone	BRT 7 Gy + PLD	MBRT 28 Gy + PLD	MBRT 100 Gy + PLD
Encapsulated plasma $AUC_{0\text{-}96h}$ (h*ng/ml)	1,521,581	1,483,098	1,347,050	1,197,501
Sum total tumor $AUC_{0\text{-}96h}$ (h*ng/g)	187,548	501,635	1,176,656	420,780
Ratio of tumor:plasma $AUC_{0\text{-}96h}$ (%)	12.33	33.82	87.35	35.14

BRT, broadbeam radiation therapy; MBRT, minibeam radiation therapy; PK, pharmacokinetics; PLD, PEGylated liposomal doxorubicin. Destructive sampling methods and groupings were used to generate the PK parameters, where the plasma and tumor concentration *versus* time values in each treatment cohort were grouped together to generate a single mean value at each time point and subsequent single PK parameter.[16,41,42] Thus, statistical comparisons could not be performed.

Table 2. Comparison of MBRT-induced delivery of PLD at 96 h after a single dose of MBRT 28 Gy in mice with different size tumors and associated PLD plasma exposures.

PK parameter	Mice with smaller than normal tumors	Mice with standard size tumors
Tumor size (mm^3)[a]	75.3 ± 0.6	210.3 ± 52.8
Encapsulated plasma concentration (ng/ml)[a]	9311 ± 2174	2079 ± 1090
Sum total tumor[a] concentration (ng/g)	110,416 ± 29,753	16,780 ± 4539
Ratio of tumor:plasma concentration[b]	11.80 ± 0.60	10.13 ± 5.88

MBRT, minibeam radiation therapy; PK, pharmacokinetics; PLD, PEGylated liposomal doxorubicin.
[a]Results are statistically different ($p < 0.05$).
[b]Results are not statistically different ($p > 0.05$).

sum total tumor doxorubicin concentration (110,416 ± 29,753 *versus* 16,780 ± 4539 ng/g), but the ratio of tumor to plasma doxorubicin concentration did not differ between the groups (11.80 ± 0.60 *versus* 10.13 ± 5.88). This suggests that the tumor delivery enhancement provided by MBRT is not limited by NP exposure in plasma across an ~4-fold range of plasma concentrations. These results also highlight the importance of keeping all aspects of the murine model and tumor consistent throughout the study. All other studies presented in this manuscript used mice with tumors between 150 to 300 mm^3.

Multiple-dose PK

After identifying enhanced tumor delivery following a single dose of MBRT 28 Gy + PLD, the efficacy of repeated dosing was investigated. The encapsulated plasma and sum total tumor doxorubicin concentration *versus* time profiles for 24 h following PLD administration for single-dose PLD alone, single-dose MBRT 28 Gy + PLD, and two-dose MBRT 28 Gy + PLD weekly are presented in Figure 3. The encapsulated plasma and sum total tumor doxorubicin $AUC_{0\text{-}24h}$ and ratio of tumor to plasma $AUC_{0\text{-}24h}$ for these treatments are presented in Table 3.

There are slight differences in the encapsulated plasma doxorubicin exposures with single-dose MBRT 28 Gy + PLD giving an $AUC_{0\text{-}24h}$ approximately 24% lower relative to PLD alone and two-dose MBRT 28 Gy + PLD 31% higher relative to PLD alone. The tumor accumulation of sum total doxorubicin is significantly enhanced following one or two doses of MBRT 28 Gy + PLD compared with PLD alone. The sum total tumor doxorubicin $AUC_{0\text{-}24h}$ are 36,710, 156,244, and 267,275 h*ng/g following a single dose of PLD alone, a single dose of MBRT 28 Gy + PLD, and two doses of MBRT 28 Gy + PLD weekly, respectively. In addition, tumor sum total doxorubicin exposure is increased following a second dose of MBRT 28 Gy + PLD

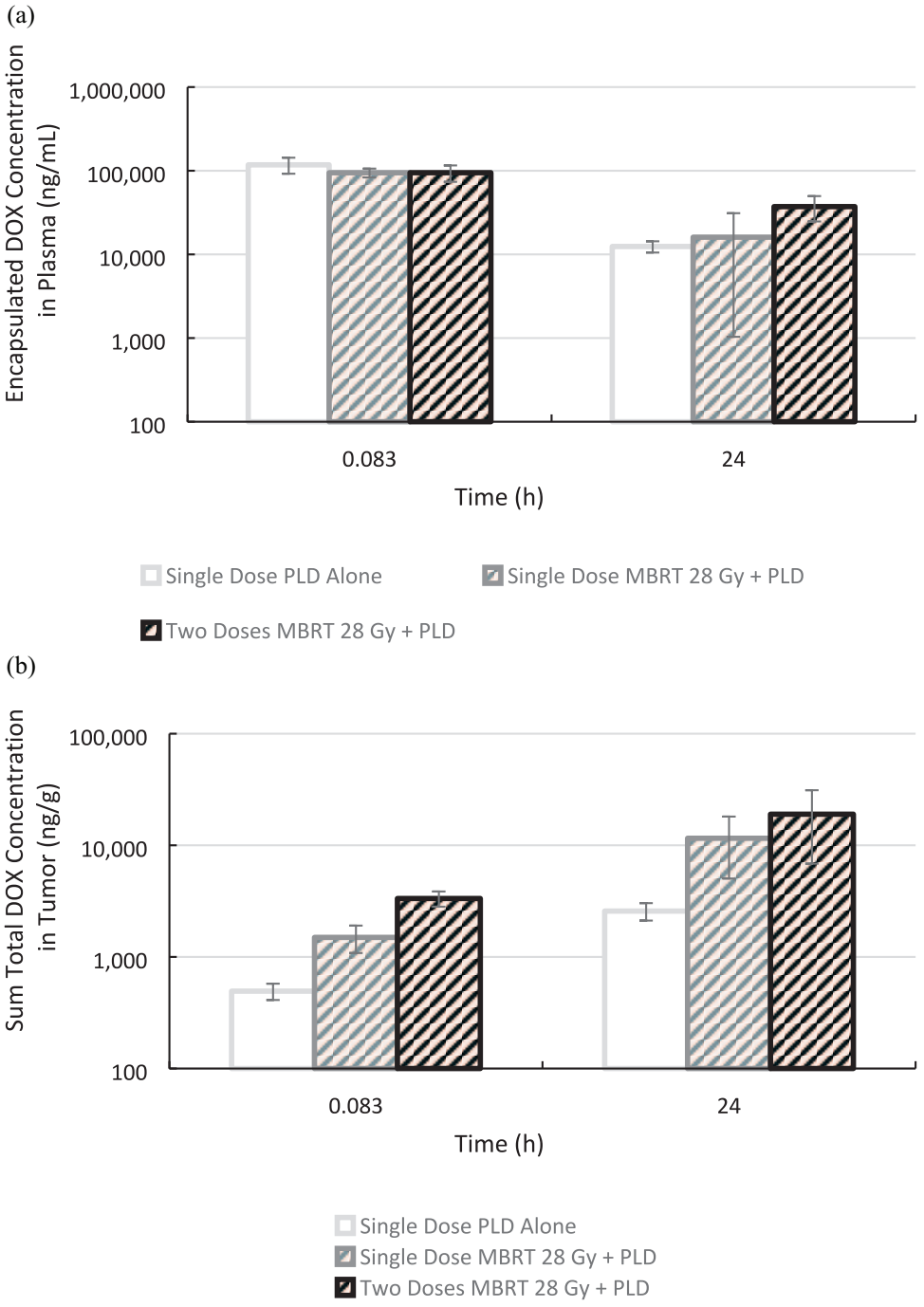

Figure 3. Mean and SD encapsulated doxorubicin concentration in plasma (a) and sum total doxorubicin concentration in tumor (b) *versus* time profiles in female T11 mice after administration of: (1) single-dose PLD alone, (2) single-dose MBRT 28 Gy + PLD, or (3) two-dose MBRT 28 Gy + PLD. The dose of PLD was 6 mg/kg IV in all groups. There was no significant difference in the plasma exposures of encapsulated doxorubicin at all time points ($p > 0.05$). At both time points, the tumor exposure of sum total doxorubicin is significantly enhanced following one and two doses of MBRT 28 Gy + PLD compared with PLD alone ($p < 0.05$). Tumor sum total doxorubicin exposure after the second dose of MBRT 28 Gy + PLD was increased relative to a single dose (at 0.083 h results were $p < 0.05$; at 24 h results were $p > 0.05$).

Table 3. Summary of PLD pharmacokinetics after a single dose of PLD alone or one or two treatments of MBRT 28 Gy + PLD weekly.

PK parameter	Single-dose PLD alone	Single treatment MBRT 28 Gy + PLD	Two treatments MBRT 28 Gy + PLD
Encapsulated plasma $AUC_{0\text{-}24h}$ (h*ng/ml)	1,129,373	854,637	1,480,638
Sum total tumor $AUC_{0\text{-}24h}$ (h*ng/g)	36,710	156,244	267,275
Ratio of tumor:plasma $AUC_{0\text{-}24h}$ (%)	3.25	18.28	18.05

MBRT, minibeam radiation therapy; PK, pharmacokinetics; PLD, PEGylated liposomal doxorubicin.
Destructive sampling methods and groupings were used to generate the PK parameters, where the plasma and tumor concentration *versus* time values in each treatment cohort were grouped together to generate a single mean value at each time point and subsequent single PK parameter.[16,41,42] Thus, statistical comparisons could not be performed.

relative to a single dose, consistent with increased plasma encapsulated doxorubicin exposure. The relative tumor delivery (given by the ratio of tumor to plasma $AUC_{0\text{-}24h}$) is similar following one (18.28%) or two (18.05%) doses of MBRT 28 Gy + PLD and higher than following a single dose of PLD alone (3.25%). The relative tumor delivery (ratio of tumor to plasma $AUC_{0\text{-}24h}$) was approximately 5.6-fold higher following either one or two doses of MBRT 28 Gy + PLD compared with PLD alone. The relative tumor delivery enhancement of PLD following MBRT is conserved following a second dose.

Tumor microenvironment profiling

The tumor microenvironment plays a pivotal role in the delivery and accumulation of NP drugs. In particular, alterations in macrophages and vasculature have been associated with changes in nanodrug delivery to tumors.[19,58,60] A separate group of T11 mice were randomized to either no radiation, BRT 7 Gy, MBRT 28 Gy, or MBRT 100 Gy and tumors were profiled via immunohistochemistry. H-scores for F4/80, Collagen IV, and MTS and microvessel density (CD31) in viable tumor are presented in Figure 4.

There is a significant, dose-dependent reduction in macrophages in viable tumor, as evidenced by decreases in F4/80 H-Scores, 24 h after both BRT and MBRT. The highest F4/80 H-score was observed in the Untreated Control group (175.3 ± 12.1) followed by the lower radiation doses, BRT 7 Gy (98.2 ± 4.3) and MBRT 28 Gy (84.4 ± 20.2). The higher peak radiation dose, MBRT 100 Gy, resulted in the lowest F4/80 H-score (27.5 ± 21.4). In this study, radiation led to depletion of macrophages in viable tumor tissue 24 h after either BRT or MBRT. Lower radiation doses, BRT 7 Gy and MBRT 28 Gy, resulted in 44% and 52% reductions in macrophages, respectively, while the higher radiation dose of MBRT 100 Gy resulted in 84% reduction in macrophages. A previous BRT study associated a relative increase in macrophages following radiation with an increase in nanodrug delivery.[57] However, the relative timing of radiotherapy and nanodrug administration differed between the two studies. Miller *et al.* administered a therapeutic polymeric cisplatin prodrug NP (TNP) 72 h post-irradiation and assessed macrophage presence 24 h post-TNP administration (96 h post-irradiation). Macrophage assessment and PLD administration in our study was performed 24 h post-irradiation. Furthermore, analytical techniques differed as macrophages were assessed relative to tumor cells in a flow cytometry assay by Miller *et al.* A potential explanation for these seemingly opposite findings would be a rapid radiation-induced nadir of macrophages (within 24 h post-irradiation) followed by later macrophage infiltration resulting in the increased PLD tumor exposure 24–96 h post-PLD (48–120 h post-irradiation). The exact mechanism(s) associated with the depletion of macrophages is unclear.

Collagen, assessed by both Collagen IV IHC and MTS, showed no significant changes between untreated control and irradiated tumors. In addition, microvessel density, assessed by CD31, also did not differ between untreated control and irradiated tumors. This suggests that, at least for the first 24 h following radiation, there is no change in collagen content or microvessel number driving the enhancement of NP delivery to tumors.

In this study, we evaluated the impact of conventional BRT in comparison to novel MBRT on the tumor microenvironment and ability to enhance tumor delivery of a drug-loaded NP. In a

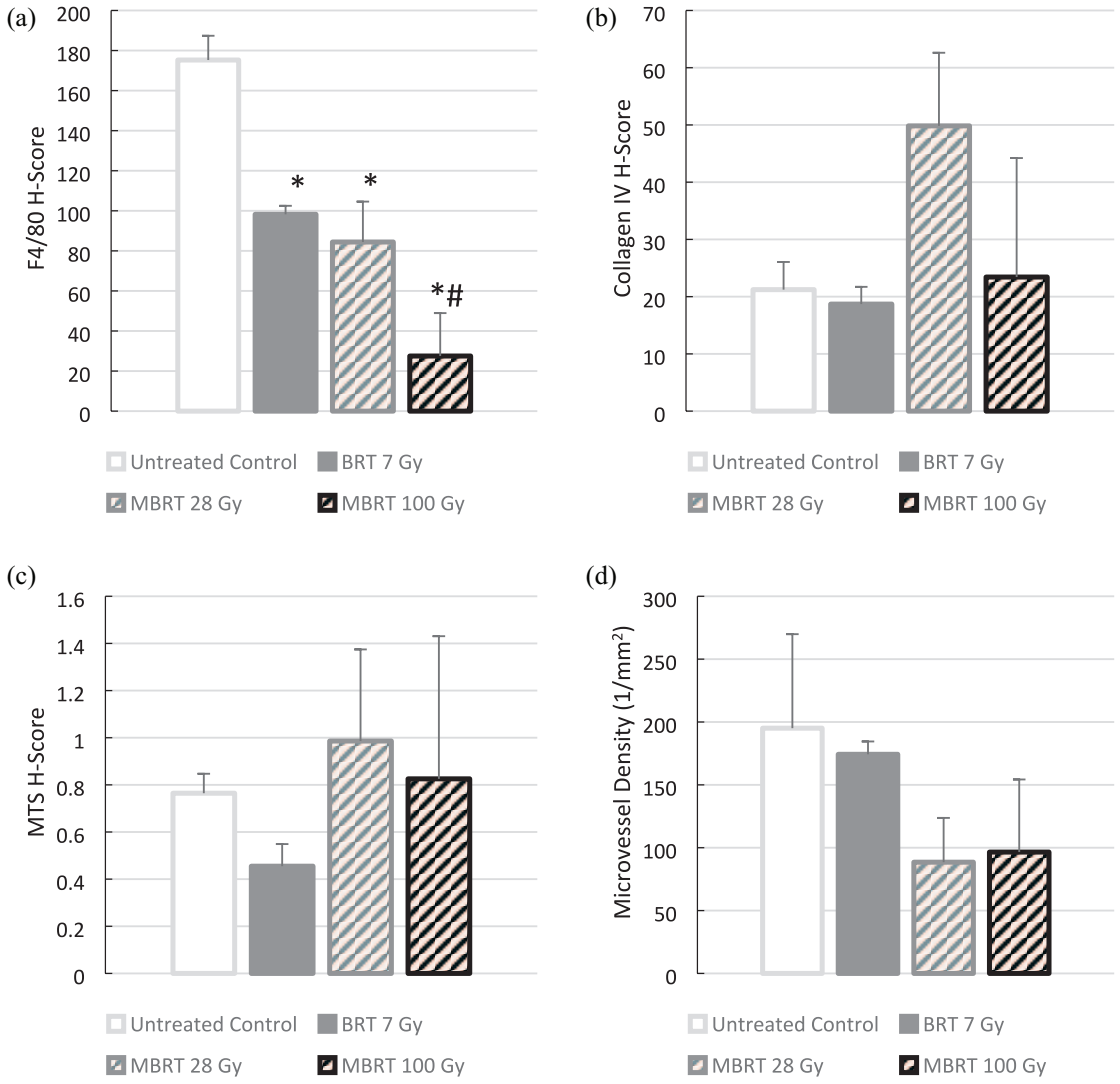

Figure 4. Tumor microenvironment profiles 24 h after (1) no radiation, (2) BRT 7 Gy, (3) MBRT 28 Gy, or (4) MBRT 100 Gy, in female T11 mice: (a) F4/80 H-scores, (b) Collagen IV H-Scores, (c) MTS H-scores, and (d) CD31 microvessel density. All results are mean and SD. *$p < 0.01$ *versus* untreated control, #$p < 0.01$ *versus* BRT 7 Gy. Both BRT and MBRT decrease macrophages with MBRT 100 Gy yielding a larger decrease in F4/80 H-scores in viable tumor. There are no statistically significant ($p > 0.05$) changes in collagen as assessed by either Collagen IV or MTS or microvessel density (CD31) between untreated control and any radiation therapy group.

genetically engineered mouse model (GEMM) of triple-negative breast cancer, both BRT and MBRT altered the microenvironment through depletion of macrophages and significantly enhanced the tumor delivery of PLD. Notably, high-dose MBRT at 100 Gy peak dose (valley dose of 7.5 Gy) provided comparable PLD tumor delivery enhancement as BRT at 7 Gy. However, the most significant enhancement of tumor delivery occurred when a lower peak radiation dose MBRT of 28 Gy (valley dose of 2.1 Gy) was used. In addition, the tumor delivery enhancement provided by pretreatment with MBRT 28 Gy is maintained at both high and low plasma exposure and following repeated dosing. Further studies are warranted to assess the efficacy of radiation-induced tumor delivery enhancement in other tumor models and with other NPs as well as the mechanism of radiation-induced tumor delivery enhancement.

Acknowledgements

The authors thank the UNC Translational Pathology Laboratory (TPL) for expert technical assistance. The UNC TPL is supported in part by grants from the NCI (2-P30-CA016086-40),

NIEHS (2-P30ES010126-15A1), UCRF, and NCBT (2015-IDG-1007). Animal histopathology was performed by the Animal Histopathology & Laboratory Medicine Core at UNC, which is supported in part by an NCI Center Core Support Grant (5P30CA016086-41) to the UNC Lineberger Comprehensive Cancer Center. The authors wish to acknowledge Certara for providing academic access to Phoenix WinNonlin through the Center of Excellence program.

Author contributions

SXC and WCZ designed and directed the project. LSLP, JNR, AJM, LBH, JAP, SM, CMS, JRR, BK, NNF, and DD performed the experiments. LSLP and JNR analyzed the data and drafted the manuscript in consultation with SXC and WCZ. All authors discussed the results and commented on the manuscript.

Conflict of interest statement

The authors declared no potential conflicts of interest with respect to the research, authorship, and/or publication of this article.

Funding

The authors disclosed receipt of the following financial support for the research, authorship, and/or publication of this article: This work was supported by the UNC Eshelman Institute for Innovation (grant number: RX03512214), the Carolina Center of Cancer Nanotechnology Excellence Pilot Grant Program (grant number: 1U54CA198999-01), and the National Cancer Institute of the National Institutes of Health (grant number: T32CA196589).

Disclaimer

This article was prepared while L.S.L.P. was employed at UNC Eshelman School of Pharmacy. Present address for L.S.L.P. is Division of Cancer Pharmacology II, Office of Clinical Pharmacology, Office of Translational Sciences, Center for Drug Evaluation and Research, US Food and Drug Administration, Silver Spring, MD, USA. The opinions expressed in this article are the author's own and do not reflect the view of the Food and Drug Administration, the Department of Health and Human Services, or the United States government.

References

1. McNeil SE. Challenges for nanoparticle characterization. *Methods Mol Biol* 2011; 697: 9–15.
2. McNeil SE. Unique benefits of nanotechnology to drug delivery and diagnostics. *Methods Mol Biol* 2011; 697: 3–8.
3. Caron WP, Song G, Kumar P, *et al*. Interpatient pharmacokinetic and pharmacodynamic variability of carrier-mediated anticancer agents. *Clin Pharmacol Ther* 2012; 91: 802–812.
4. Prabhakar U, Maeda H, Jain RK, *et al*. Challenges and key considerations of the enhanced permeability and retention effect for nanomedicine drug delivery in oncology. *Cancer Res* 2013; 73: 2412–2417.
5. Zamboni WC, Torchilin V, Patri AK, *et al*. Best practices in cancer nanotechnology: perspective from NCI nanotechnology alliance. *Clin Cancer Res* 2012; 18: 3229–3241.
6. Chauhan VP, Stylianopoulos T, Boucher Y, *et al*. Delivery of molecular and nanoscale medicine to tumors: transport barriers and strategies. *Annu Rev Chem Biomol Eng* 2011; 2: 281–298.
7. Jain RK and Stylianopoulos T. Delivering nanomedicine to solid tumors. *Nat Rev Clin Oncol* 2010; 7: 653–664.
8. Diop-Frimpong B, Chauhan VP, Krane S, *et al*. Losartan inhibits collagen I synthesis and improves the distribution and efficacy of nanotherapeutics in tumors. *Proc Natl Acad Sci USA* 2011; 108: 2909–2914.
9. Jain RK. Normalizing tumor microenvironment to treat cancer: bench to bedside to biomarkers. *J Clin Oncol* 2013; 31: 2205–2218.
10. Liu J, Liao S, Diop-Frimpong B, *et al*. TGF-beta blockade improves the distribution and efficacy of therapeutics in breast carcinoma by normalizing the tumor stroma. *Proc Natl Acad Sci USA* 2012; 109: 16618–16623.
11. Maeda H, Nakamura H and Fang J. The EPR effect for macromolecular drug delivery to solid tumors: improvement of tumor uptake, lowering of systemic toxicity, and distinct tumor imaging in vivo. *Adv Drug Deliv Rev* 2013; 65: 71–79.
12. Raut CP, Boucher Y, Duda DG, *et al*. Effects of sorafenib on intra-tumoral interstitial fluid pressure and circulating biomarkers in patients with refractory sarcomas (NCI protocol 6948). *PLoS ONE* 2012; 7: e26331.
13. Chu KS, Hasan W, Rawal S, *et al*. Plasma, tumor and tissue pharmacokinetics of Docetaxel delivered via nanoparticles of different sizes and shapes in mice bearing SKOV-3 human ovarian carcinoma xenograft. *Nanomedicine* 2013; 9: 686–693.
14. Jain RK, Munn LL and Fukumura D. Measuring vascular permeability in mice. *Cold Spring Harb Protoc* 2013; 2013: 444–446.

15. Madden AJ, Rawal S, Sandison K, *et al*. Evaluation of the efficiency of tumor and tissue delivery of carrier-mediated agents (CMA) and small molecule (SM) agents in mice using a novel pharmacokinetic (PK) metric: relative distribution index over time (RDI-OT). *J Nanopart Res* 2014; 16: 2662.

16. Song G, Darr DB, Santos CM, *et al*. Effects of tumor microenvironment heterogeneity on nanoparticle disposition and efficacy in breast cancer tumor models. *Clin Cancer Res* 2014; 20: 6083–6095.

17. Stylianopoulos T, Martin JD, Snuderl M, *et al*. Coevolution of solid stress and interstitial fluid pressure in tumors during progression: implications for vascular collapse. *Cancer Res* 2013; 73: 3833–3841.

18. Walsh MD, Hanna SK, Sen J, *et al*. Pharmacokinetics and antitumor efficacy of XMT-1001, a novel, polymeric topoisomerase I inhibitor, in mice bearing HT-29 human colon carcinoma xenografts. *Clin Cancer Res* 2012; 18: 2591–2602.

19. Zamboni WC, Eiseman JL, Strychor S, *et al*. Tumor disposition of pegylated liposomal CKD-602 and the reticuloendothelial system in preclinical tumor models. *J Liposome Res* 2011; 21: 70–80.

20. Parrott MC, Luft JC, Byrne JD, *et al*. Tunable bifunctional silyl ether cross-linkers for the design of acid-sensitive biomaterials. *J Am Chem Soc* 2010; 132: 17928–17932.

21. Rolland JP, Maynor BW, Euliss LE, *et al*. Direct fabrication and harvesting of monodisperse, shape-specific nanobiomaterials. *J Am Chem Soc* 2005; 127: 10096–10100.

22. Gabizon A, Bradbury M, Prabhakar U, *et al*. Cancer nanomedicines: closing the translational gap. *Lancet* 2014; 384: 2175–2176.

23. Tyldesley S, Delaney G, Foroudi F, *et al*. Estimating the need for radiotherapy for patients with prostate, breast, and lung cancers: verification of model estimates of need with radiotherapy utilization data from British Columbia. *Int J Radiat Oncol Biol Phys* 2011; 79: 1507–1515.

24. Fernandez-Palomo C, Schultke E, Brauer-Krisch E, *et al*. Investigation of abscopal and bystander effects in immunocompromised mice after exposure to pencilbeam and microbeam synchrotron radiation. *Health Phys* 2016; 111: 149–159.

25. Fontanella AN, Boss MK, Hadsell M, *et al*. Effects of high-dose microbeam irradiation on tumor microvascular function and angiogenesis. *Radiat Res* 2015; 183: 147–158.

26. Sedelnikova OA, Nakamura A, Kovalchuk O, *et al*. DNA double-strand breaks form in bystander cells after microbeam irradiation of three-dimensional human tissue models. *Cancer Res* 2007; 67: 4295–4302.

27. Brauer-Krisch E, Serduc R, Siegbahn EA, *et al*. Effects of pulsed, spatially fractionated, microscopic synchrotron X-ray beams on normal and tumoral brain tissue. *Mutat Res* 2010; 704: 160–166.

28. Griffin RJ, Koonce NA, Dings RP, *et al*. Microbeam radiation therapy alters vascular architecture and tumor oxygenation and is enhanced by a galectin-1 targeted anti-angiogenic peptide. *Radiat Res* 2012; 177: 804–812.

29. Griffin R, Ahmed MM, Amendola BE, *et al*. Understanding high-dose, ultra-high dose-rate and spatially fractionated radiotherapy. *Int J Radiat Oncol Biol Phys* 2020; 107: 766–778.

30. Guardiola C, Peucelle C and Prezado Y. Optimization of the mechanical collimation for minibeam generation in proton minibeam radiation therapy. *Med Phys* 2017; 44: 1470–1478.

31. Fernandez-Palomo C, Fazzari J, Trappetti V, *et al*. Animal models in microbeam radiation therapy: a scoping review. *Cancers* 2020; 12: 527.

32. Choi JI, Daniels J, Cohen D, *et al*. Clinical outcomes of spatially fractionated GRID radiotherapy in the treatment of bulky tumors of the head and neck. *Cureus* 2019; 11: e4637.

33. Mohiuddin M, Fujita M, Regine WF, *et al*. High-dose spatially-fractionated radiation (GRID): a new paradigm in the management of advanced cancers. *Int J Radiat Oncol Biol Phys* 1999; 45: 721–727.

34. Blanco Suarez JM, Amendola BE, Perez N, *et al*. The use of lattice radiation therapy (LRT) in the treatment of bulky tumors: a case report of a large metastatic mixed mullerian ovarian tumor. *Cureus* 2015; 7: e389.

35. Mohiuddin M, Lynch C, Gao M, *et al*. Early clinical results of proton spatially fractionated GRID radiation therapy (SFGRT). *Br J Radiol* 2020; 93: 20190572.

36. Rivera JN, Kierski TM, Kasoji SK, *et al*. Conventional dose rate spatially-fractionated radiation therapy (SFRT) treatment response and its association with dosimetric parameters—a preclinical study in a Fisher 344 rat model. *PLoS ONE* 2020; 15: e0229053.

37. Fernandez-Palomo C, Brauer-Krisch E, Laissue J, *et al*. Use of synchrotron medical microbeam irradiation to investigate radiation-induced bystander and abscopal effects in vivo. *Phys Med* 2015; 31: 584–595.

38. Pfefferle AD, Herschkowitz JI, Usary J, *et al*. Transcriptomic classification of genetically engineered mouse models of breast cancer identifies human subtype counterparts. *Genome Biol* 2013; 14: R125.

39. Usary J, Darr DB, Pfefferle AD, *et al*. Overview of genetically engineered mouse models of distinct breast cancer subtypes. *Curr Protoc Pharmacol* 2016; 72: 14.38.1–14.38.11.

40. Herschkowitz JI, Zhao W, Zhang M, *et al*. Comparative oncogenomics identifies breast tumors enriched in functional tumor-initiating cells. *Proc Natl Acad Sci USA* 2012; 109: 2778–2783.

41. Merkel TJ, Chen K, Jones SW, *et al*. The effect of particle size on the biodistribution of low-modulus hydrogel PRINT particles. *J Control Release* 2012; 162: 37–44.

42. Song G, Suzuki OT, Santos CM, *et al*. Gulp1 is associated with the pharmacokinetics of PEGylated liposomal doxorubicin (PLD) in inbred mouse strains. *Nanomedicine* 2016; 12: 2007–2017.

43. Amselem S, Gabizon A and Barenholz Y. Optimization and upscaling of doxorubicin-containing liposomes for clinical use. *J Pharm Sci* 1990; 79: 1045–1052.

44. Anders CK, Adamo B, Karginova O, *et al*. Pharmacokinetics and efficacy of PEGylated liposomal doxorubicin in an intracranial model of breast cancer. *PLoS ONE* 2013; 8: e61359.

45. Gabizon A, Shiota R and Papahadjopoulos D. Pharmacokinetics and tissue distribution of doxorubicin encapsulated in stable liposomes with long circulation times. *J Natl Cancer Inst* 1989; 81: 1484–1488.

46. Petschauer JS, Madden AJ, Kirschbrown WP, *et al*. The effects of nanoparticle drug loading on the pharmacokinetics of anticancer agents. *Nanomedicine* 2015; 10: 447–463.

47. Zamboni WC, Strychor S, Joseph E, *et al*. Plasma, tumor, and tissue disposition of STEALTH liposomal CKD-602 (S-CKD602) and nonliposomal CKD-602 in mice bearing A375 human melanoma xenografts. *Clin Cancer Res* 2007; 13: 7217–7223.

48. Budwit-Novotny DA, McCarty KS, Cox EB, *et al*. Immunohistochemical analyses of estrogen receptor in endometrial adenocarcinoma using a monoclonal antibody. *Cancer Res* 1986; 46: 5419–5425.

49. Nedelman JR, Gibiansky E and Lau DT. Applying Bailer's method for AUC confidence intervals to sparse sampling. *Pharm Res* 1995; 12: 124–128.

50. Vickers AJ. The use of percentage change from baseline as an outcome in a controlled trial is statistically inefficient: a simulation study. *BMC Med Res Methodol* 2001; 1: 6.

51. Ambady P, Wu YJ, Walker JM, *et al*. Enhancing the cytotoxicity of chemoradiation with radiation-guided delivery of anti-MGMT morpholino oligonucleotides in non-methylated solid tumors. *Cancer Gene Ther* 2017; 24: 348–357.

52. Davies CDL, Lundstrom LM, Frengen J, *et al*. Radiation improves the distribution and uptake of liposomal doxorubicin (caelyx) in human osteosarcoma xenografts. *Cancer Res* 2004; 64: 547–553.

53. Giustini AJ, Petryk AA and Hoopes PJ. Ionizing radiation increases systemic nanoparticle tumor accumulation. *Nanomedicine* 2012; 8: 818–821.

54. Lammers T, Peschke P, Kuhnlein R, *et al*. Effect of radiotherapy and hyperthermia on the tumor accumulation of HPMA copolymer-based drug delivery systems. *J Control Release* 2007; 117: 333–341.

55. Lammers T, Subr V, Peschke P, *et al*. Image-guided and passively tumour-targeted polymeric nanomedicines for radiochemotherapy. *Br J Cancer* 2008; 99: 900–910.

56. Li C, Ke S, Wu QP, *et al*. Tumor irradiation enhances the tumor-specific distribution of poly(L-glutamic acid)-conjugated paclitaxel and its antitumor efficacy. *Clin Cancer Res* 2000; 6: 2829–2834.

57. Miller MA, Chandra R, Cuccarese MF, *et al*. Radiation therapy primes tumors for nanotherapeutic delivery via macrophage-mediated vascular bursts. *Sci Transl Med* 2017; 9: eaal0225.

58. Kai MP, Brighton HE, Fromen CA, *et al*. Tumor presence induces global immune changes and enhances nanoparticle clearance. *ACS Nano* 2016; 10: 861–870.

59. Song G, Tarrant TK, White TF, *et al*. Roles of chemokines CCL2 and CCL5 in the pharmacokinetics of PEGylated liposomal doxorubicin in vivo and in patients with recurrent epithelial ovarian cancer. *Nanomedicine* 2015; 11: 1797–1807.

60. Lucas AT, White TF, Deal AM, *et al*. Profiling the relationship between tumor-associated macrophages and pharmacokinetics of liposomal agents in preclinical murine models. *Nanomedicine* 2017; 13: 471–482.